Chemical Science

ROYAL SOCIETY OF CHEMISTRY

EDGE ARTICLE

View Article Online
View Journal | View Issue

Check for updates

Cite this: *Chem. Sci.*, 2024, **15**, 17950

All publication charges for this article have been paid for by the Royal Society of Chemistry

Received 27th July 2024
Accepted 5th October 2024

DOI: 10.1039/d4sc05006a

rsc.li/chemical-science

Quadrupolar dinuclear hypervalent tin(IV) compounds with near-infrared emission consisting of Schiff bases based on π-conjugated scaffolds†

Kazuya Tanimura, [a] Kento Tanaka, [a] Masayuki Gon [ab] and Kazuo Tanaka *[ab]

Since π-conjugated molecules are commonly used as a scaffold for constructing optoelectronic and functional materials, much effort has been devoted to exploring novel molecular scaffolds for obtaining superior properties. This study focuses on dinuclear hypervalent tin(IV) compounds prepared by the ladderization of Schiff bases using hypervalent tin units. The optical measurements found that introducing hypervalent tin atoms can reinforce the D–π–A system. We synthesized two types of dinuclear hypervalent compounds by simple condensation reactions and observed near-infrared (NIR) emission. Also, depending on the direction of the imine bonds, these molecules had different quadrupolar orientations with D–π–A–π–D and A–π–D–π–A systems followed by negative solvatochromism, which is the unique behavior of quadrupolar-derived absorption. Furthermore, the π-conjugated polymers involving dinuclear compounds showed NIR emission in the wavelength range over 800 nm owing to the distinct expansion of π-conjugation. Our findings could be useful not only for constructing electronic structures with narrow energy gaps but also for designing molecules with unique electronic states and environmental responsiveness.

Open Access Article. Published on 10 October 2024. Downloaded on 2/15/2026 8:28:08 PM. This article is licensed under a Creative Commons Attribution-NonCommercial 3.0 Unported Licence.

Introduction

Conjugated molecules have attracted significant interest because of their unique optical and electronic properties and wide range of applicability, especially in materials science,[1–4] biomedical science[5] and environmental sensing.[6] Among the various designs of π-conjugated structures, ladder molecules with fused π-conjugated backbones exhibit intriguing optical and physical properties for functional materials because of their rigid structures.[7] The ladderization methods have extended beyond basic carbon and have been widely studied using heteroatoms.[8] In π-conjugated scaffolds with the ladder-like structures linked by heteroatoms, electronic interactions between the heteroatoms and the π-conjugated system have resulted in unique optical properties and various characteristics derived from the hetero elements that are not present in carbon-based fused rings.[9,10] To fulfill the requirements for creating advanced materials with high stability, good processability, and tunable optical properties, it is significant to explore new molecular frameworks for constructing ladder π-conjugated compounds and elucidate their optical and electronic properties.

We have been studying the "hypervalent state"[11] created by main-group elements for constructing a ladder skeleton based on heteroatoms. The hypervalent states are regarded as multi-coordinate species that formally have electrons exceeding the octet rule, and many researchers have focused on their synthesis, geometry, and reactivity.[12–15] Our previous reports have looked at the unique electronic states of the hypervalent state to modify the electronic structure of π-conjugated scaffolds.[16] Main group elements like tin,[17–21] germanium[22,23] and bismuth[24] in the hypervalent state are suggested to create coordination position-specific electronic effects on π-conjugated molecules through the intermolecular Lewis D–A interaction at the equatorial position and the polarized bond known as three-center/four-electron (3c–4e) bonds at the apical position. Based on these site-specific electronic properties, we obtained NIR materials without significantly increasing the molecular size and finally obtained polymers that can exhibit NIR absorption and/or emission properties.[16,18,22,25] This strategy offers a new way to control the electronic properties of π-conjugated scaffolds by creating unique inductive effects related to the hypervalent state.

In this study, we created a series of hypervalent tin compounds by the ladderization of Schiff bases (also known as azomethines) using hypervalent tin units. Specifically, we observed both negative solvatochromic behaviors and NIR emission with small π-conjugated structures through the

[a]*Department of Polymer Chemistry, Graduate School of Engineering, Kyoto University, Katsura, Nishikyo-ku, Kyoto 615-8510, Japan. E-mail: tanaka@poly.synchem.kyoto-u.ac.jp*

[b]*Department of Technology and Ecology, Graduate School of Global Environmental Studies, Kyoto University, Katsura, Nishikyo-ku, Kyoto 615-8510, Japan*

† Electronic supplementary information (ESI) available: Experimental details "bisTPh_SI.pdf". CCDC 2373875 and 2373876. For ESI and crystallographic data in CIF or other electronic format see DOI: https://doi.org/10.1039/d4sc05006a

© 2024 The Author(s). Published by the Royal Society of Chemistry

Open Access Article. Published on 10 October 2024. Downloaded on 2/15/2026 8:28:08 PM. This article is licensed under a Creative Commons Attribution-NonCommercial 3.0 Unported Licence.

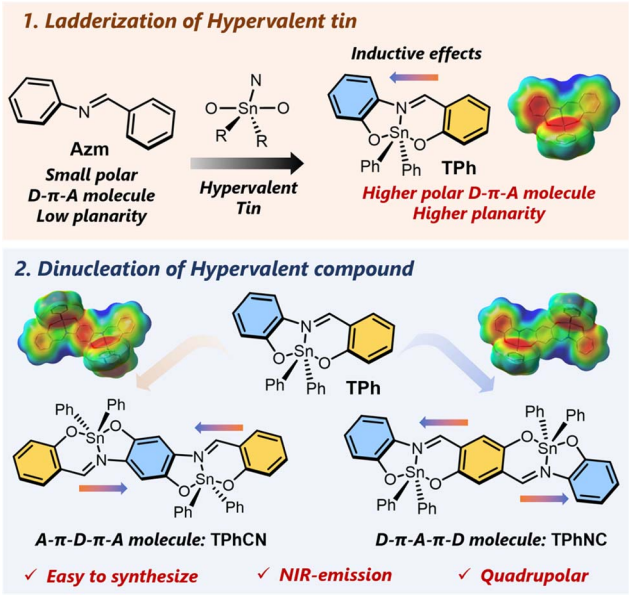

Fig. 1 Chemical structures of the Schiff base **Azm**, the mononuclear hypervalent tin compound **TPh**, and the dinuclear hypervalent tin compounds **TPhCN** and **TPhNC**.

process of dinucleation (see Fig. 1). Firstly, as previously reported with mononuclear hypervalent tin derivatives, we also evaluated the electronic effect of the introduction of hypervalent tin into the π-conjugated system by comparing the electronic states of the standard Schiff base **Azm** and the hypervalent compound **TPh**. Secondly, as mentioned above, we confirmed that hypervalent tin was able to perturb the electronic state of the π-conjugated scaffolds through different site-specific electronic interactions at the equatorial and axial positions. Furthermore, we also found that the hypervalent tin enhanced the electron-withdrawing ability of the imine moiety, and consequently, charge separation followed by the D–π–A structure was efficiently formed. Next, we synthesized two dinuclear compounds, **TPhCN** and **TPhCN**, where the direction of the imine bond is opposite, and evaluated their optical properties. Interestingly, we discovered unique optical properties such as negative solvatochromism originating from "symmetry-breaking"[26] in the ground state on the electronic structures of D–π–A–π–D or A–π–D–π–A, depending on the different quadrupolar orientation of the imine bond. We were also able to introduce each dinuclear compound into a π-conjugated polymer and obtain NIR-emitting materials having emission wavelengths over 800 nm by extending the π-conjugation and electronic interactions with the copolymer. Our findings demonstrate that hypervalent tin compounds, π-conjugated molecules bridged by hypervalent atoms, can be a new platform for developing D–A materials.

Results and discussion

Synthesis and characterization

According to the synthetic procedures reported by Peon *et al.*, **TPh** and **TPhBr** were prepared, respectively.[27] Based on the synthesis of the dinuclear boron azomethine complexes,[28] the series of azomethine ligands for dinuclear compounds (**NC**, **NCBr**, **CN**, and **CNBr**) were prepared through the imine condensation reaction (Scheme 1). The introduction of tin, followed by the formation of the hypervalent state, was achieved by refluxing with the ligands and diphenyltin(IV) oxide in acetone. After reprecipitation, the pure products were obtained in high isolated yields. We confirmed that the expected structures were obtained from characterization data from ^{1}H, ^{13}C $\{^{1}$H$\}$, ^{119}Sn NMR spectroscopy, mass spectrometry (MS), and elemental analysis. From fewer changes in time courses of UV-vis absorption spectra (1.0×10^{-5} M in toluene), it is suggested that **TPh**, **TPhCN**, and **TPhNC** should be stable under ambient conditions (Fig. S1(a)–(c)†). The photostability of each compound under strong light irradiation was also investigated

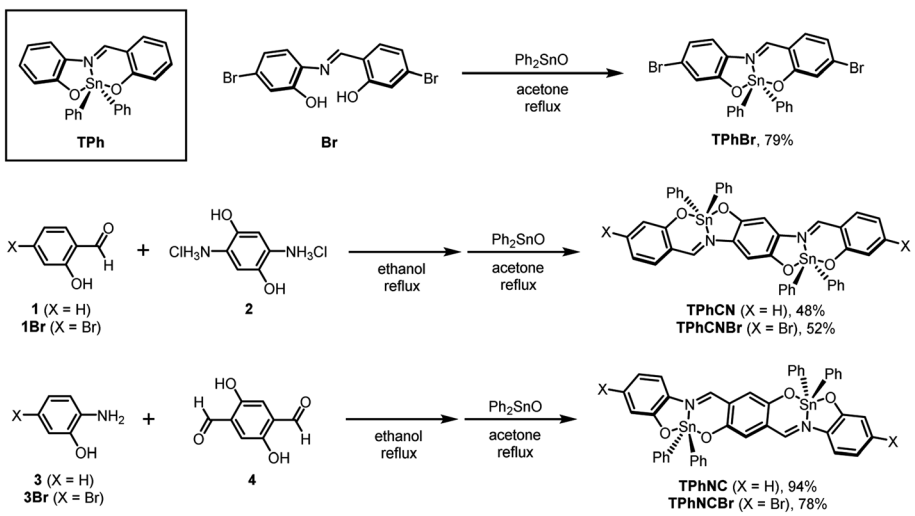

Scheme 1 Synthesis of mononuclear (**TPhBr**) and dinuclear (**TPhCN**, **TPhCNBr**, **TPhNC**, and **TPhNCBr**) hypervalent tin compounds. A chemical structure of the mononuclear compound **TPh** was also shown.

Open Access Article. Published on 10 October 2024. Downloaded on 2/15/2026 8:28:08 PM. This article is licensed under a Creative Commons Attribution-NonCommercial 3.0 Unported Licence.

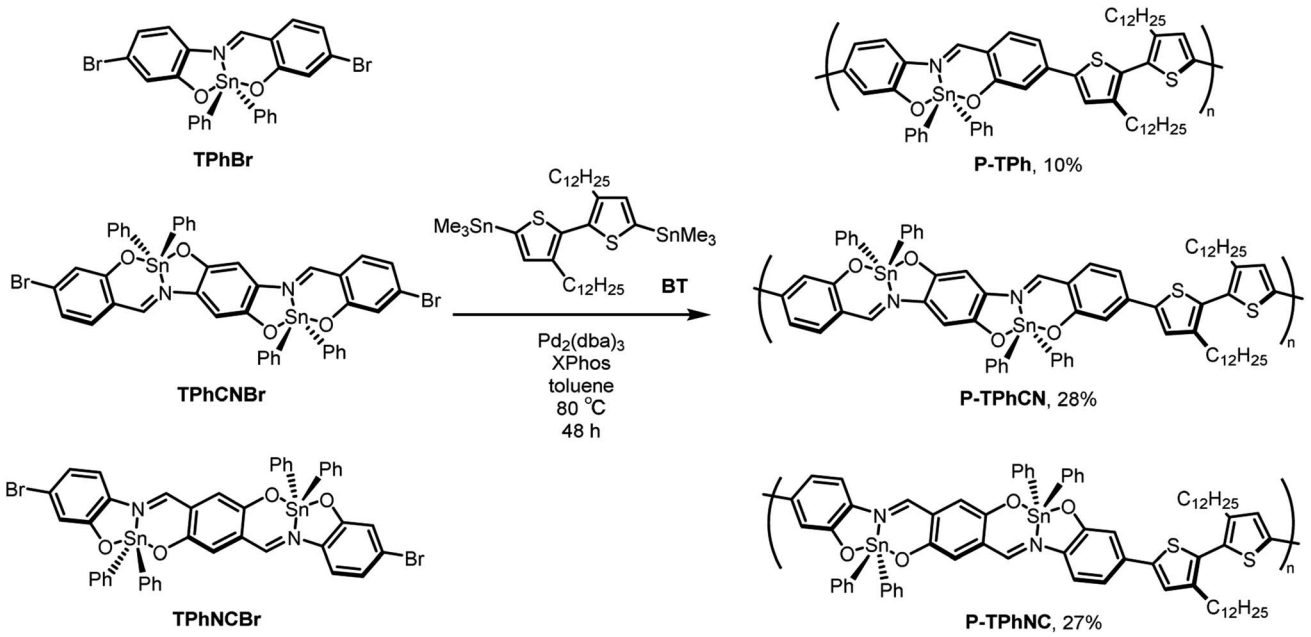

Scheme 2 Synthesis of π-conjugated polymers, P-TPh, P-TPhNC, and P-TPhCN.

by trans-illuminator (365 nm, 6500 μW cm^{-2}, 60 s) as shown in Fig. S1(d)–(f).† As a result of the absorption measurements, no changes were observed for **TPh**, whereas photodegradation was partially observed from the dinuclear compounds.

Next, we synthesized π-conjugated polymers from mononuclear and dinuclear hypervalent tin compounds by the Migita–Kosugi–Stille cross-coupling reaction (Scheme 2). **TPhBr**, **TPhCNBr**, and **TPhNCBr** were polymerized with bithiophene comonomers, and insoluble high molecular weight polymers and low molecular weight oligomers were removed by Soxhlet extraction. Regarding relative molecular weights measured by gel permeation chromatography (GPC) with polystyrene standards, the number of molecular weights (M_n) was estimated to be 4.1×10^3 for **P-TPh**, 1.8×10^4 for **P-TPhCN**, and 1.3×10^4 for **P-TPhNC**. The characterization was carried out by ^{1}H, ^{13}C{^{1}H}, ^{119}Sn NMR spectroscopy, and matrix-assisted laser desorption/ionization time of flight (MALDI-TOF) MS (see the ESI† for more details). The observed changes in absorption spectra over time for each compound did not show any noticeable changes (Fig. S2†). This indicates that each compound is sufficiently stable under the measurement conditions.

Structural features of tin compounds

The crystal structures of the mononuclear and dinuclear compounds were determined through single-crystal X-ray structure analysis (Fig. 2, S3 and S4†). Diamantis *et al.* have already reported the crystal structure of **TPh**,[29] and we referred to their structure to compare the mononuclear and dinuclear compounds. To quantitatively evaluate 5-coordinate geometries in hypervalent states, a geometry index known as the τ_5 value is often used ($\tau_5 = (\beta - \alpha)/60$. The coordination center of a molecule can have different shapes depending on its angles. The two largest angles are called β and α. When τ_5 is close to 0, the geometry is similar to square pyramidal, while if τ_5 is close to 1, the geometry is similar to trigonal bipyramidal).[30] The τ_5 value of each compound was calculated to be 0.65 for **TPh**, 0.65 for **TPhCN**, and 0.40 for **TPhNC** (**TPhNC** had asymmetric and disordered structures, and their τ_5 values were estimated to be 0.46 and 0.29) (Fig. 2). Thus, **TPh** and **TPhCN** formed distorted trigonal bipyramidal geometries, whereas **TPhNC** displayed a distorted square pyramidal one. Moreover, the torsion angles of C–C=N–C were assessed as 179.7(6)° for **TPh**, 179(1)° for **TPhCN**, and 178.3(9)° (178.0(9)°) for **TPhNC**, indicating that this dinucleation hardly affects the planarity of the molecule. On the contrary, the structural optimization of each compound in quantum chemical calculations with density functional theory (DFT) showed that all the molecules adopted trigonal bipyramidal geometries (τ_5 value of **TPh**: 0.58, **TPhCN**: 0.57, **TPhNC**: 0.57) and exhibited highly planar structures (the torsion angles of C–C=N–C in **TPh**: 177.64°, **TPhCN**: 178.09°, **TPhNC**: 177.94°) (Fig. 2). From the viewpoint of the packing, the interplane distances of the nearest-neighbor aromatic rings were 4.216 Å for **TPhCN** and 4.016 Å for **TPhNC**. These results propose that weak intermolecular interactions could be formed in the crystalline packing (Fig. S3 and S4†). In addition, these data suggest that the structures around the hypervalent tin are flexible and distorted in the crystal due to the dense packing.

Formation of hypervalent states

The formation of hypervalent states can be confirmed by the distribution of molecular orbitals (MOs) obtained from DFT calculations. In general, it is known that hypervalent states consist of three types of orbitals in apical positions: bonding, non-bonding, and antibonding orbitals, originating from a 3c–4e bond. Correspondingly, according to the distribution of the

 © 2024 The Author(s). Published by the Royal Society of Chemistry

Open Access Article. Published on 10 October 2024. Downloaded on 2/15/2026 8:28:08 PM. This article is licensed under a Creative Commons Attribution-NonCommercial 3.0 Unported Licence.

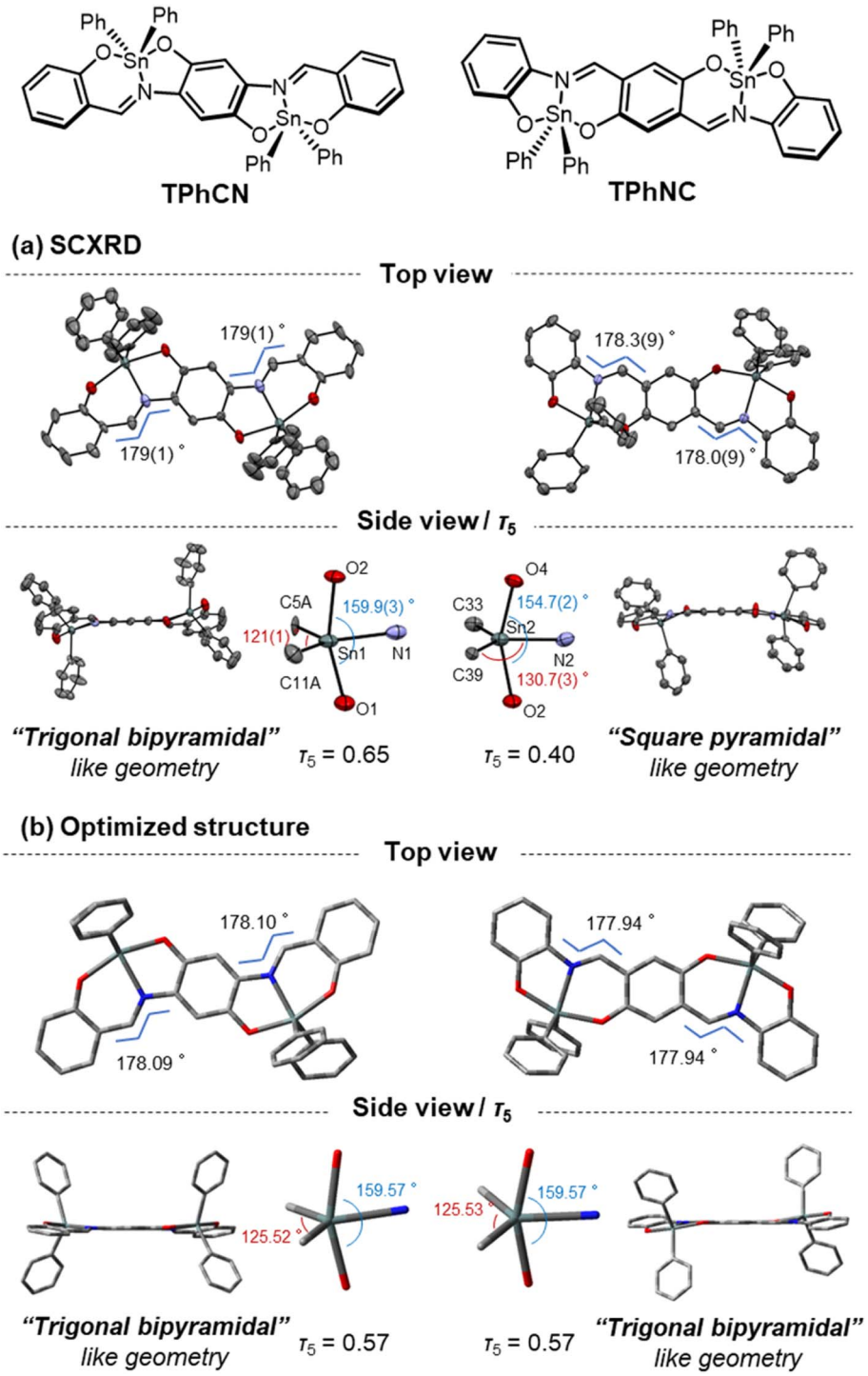

Fig. 2 (a) ORTEP drawings of the hypervalent tin compounds, **TPhCN** and **TPhNC** (50% probability for thermal ellipsoids). Hydrogens and disordered atoms were omitted to clarify. All crystallographic data are shown in ESI.† (b) Geometrical optimized structures of **TPhCN** and **TPhNC** (gray carbon atoms; red oxygen atoms; blue atom nitrogen; pale green tin atoms; hydrogen atoms are omitted for clarity) (B3LYP/6-31G(d) for C, H, N, O and LanL2DZ for Sn).

MOs for **TPh**, it was found that bonding, non-bonding, and anti-bonding orbitals should be assigned to HOMO−10, HOMO−7, and LUMO+11 and +13, respectively (Fig. S5†). Furthermore, natural bonding orbital (NBO) calculations also supported the presence of the significant bond between tin and nitrogen atoms and the corresponding orbitals constituting the 3c–4e bond on each atom (Fig. S6†). From the above data, it is expected that the tin in **TPh** forms the hypervalent state, which should have a coordination position-specific electronic effect on the π-conjugated scaffolds.

Open Access Article. Published on 10 October 2024. Downloaded on 2/15/2026 8:28:08 PM.
This article is licensed under a Creative Commons Attribution-NonCommercial 3.0 Unported Licence.

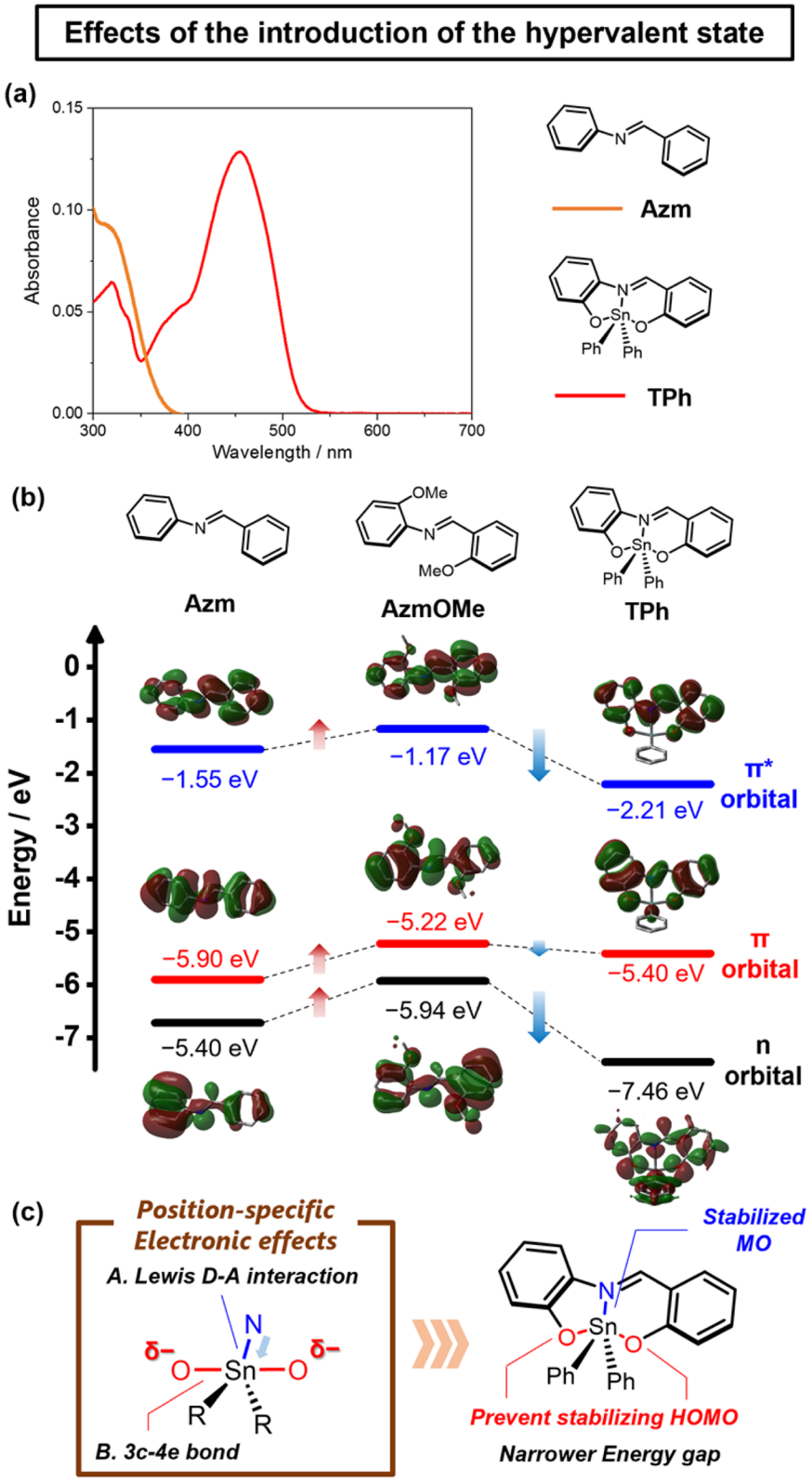

Fig. 3 (a) UV-vis absorption spectra of **Azm** and **TPh** in toluene (1.0×10^{-5} M). (b) Energy diagrams selected MOs of **Azm**, **AzmOMe**, and **TPh** obtained with TD-DFT calculations at TD-B3LYP/6-31G(d) level for C, H, N, O, and LanL2DZ for Sn (isovalue = 0.02). (c) Schematic illustration of the electronic effects of hypervalent tin.

© 2024 The Author(s). Published by the Royal Society of Chemistry

Open Access Article. Published on 10 October 2024. Downloaded on 2/15/2026 8:28:08 PM. This article is licensed under a Creative Commons Attribution-NonCommercial 3.0 Unported Licence.

To assess the electronic effects of the formation of the hypervalent state, UV-vis absorption spectra of **TPh** and the model compound **Azm** were measured in toluene (1.0×10^{-5} M), as shown in Fig. 3a. The absorption band of **TPh** was bathochromically shifted compared to that of **Azm**. The DFT calculations were performed to gain deep insight into the origin of the electronic states in the hypervalent tin derivatives (Fig. 3b and Tables S3–S6†). We evaluated the electronic effects of the hypervalent state on the π-conjugated scaffolds by comparing model compounds **Azm** and **AzmOMe**. According to the MOs of **Azm**, **AzmOMe**, and **TPh**, the LUMO energy levels were significantly stabilized by the tin coordination compared with the HOMO energy levels (**Azm**: HOMO = −5.90 eV, LUMO = −1.55 eV, **AzmOMe**: HOMO = −5.22 eV, LUMO = −1.17 eV, **TPh**: HOMO = −5.40 eV, LUMO = −2.21 eV). This result suggests that the MO is stabilized by electron-accepting nitrogen–tin (N–Sn) coordination at the equatorial position. Moreover, the stabilization of the HOMO energy level is relatively suppressed by the electron-donating 3c–4e bond, as described in our previous report (Fig. 3c).[17] The hypervalent states can exhibit electronic effects specific to their coordination positions, irrespective of ligand structures.

The distributions of electric charges and dipole moments before and after introducing the hypervalent tin were also examined using DFT calculations. From Fig. S7,† it was found that the unsymmetrical distribution of electric charges was observed from the surface of molecular electrostatic potential (MEP) of **TPh** compared with **Azm** and **AzmOMe**, and a larger degree of negative charge was observed from the benzene ring of the N-side than that of the C-side, like D–π–A molecules. These results represent that the introduction of the hypervalent tin atom should induce charge separation and reinforce the inductive effect of the imine bond. This is because of the enhanced electron-withdrawing ability by the coordination of the tin atom, which works as the Lewis acid. In addition, the dipole moment of **Azm** was 1.431 debye along the direction of the imine bond, while that of **TPh** was 2.778 debye, indicating that the asymmetric electronic state should be realized (Fig. S7†). These data suggest that the different electronic states should be realized in both dinuclear compounds where only the nitrogen position is different.

Optical and electronic properties of dinuclear compounds

UV-vis absorption and photoluminescence spectra were measured in toluene (1.0×10^{-5} M) to compare the electronic structures of dinuclear hypervalent tin compounds **TPhNC** and **TPhCN**. Fig. 4a, b and Table 1 illustrate that **TPh** exhibited the absorption band around 400–500 nm, whereas **TPhNC** and **TPhCN** displayed the absorption bands around 550–650 nm. In addition, the emission bands of dinuclear hypervalent tin compounds were bathochromically shifted compared to that of **TPh**. This implies that the dinucleation contributes to extending the π-conjugation through the imine moieties. Compared **TPhNC** with **TPhCN**, the maximum absorption wavelength of **TPhCN** (λ_{abs}^{max} = 604 nm) was longer than that of **TPhNC** (λ_{abs}^{max} = 632 nm), and the molar extinction coefficient of **TPhCN** ($\varepsilon_{abs} = 2.68 \times 10^4$ cm^{-1} M^{-1}) was larger than that of **TPhNC** ($\varepsilon_{abs} = 1.61 \times 10^4$ cm^{-1} M^{-1}). Moreover, both maxima in the fluorescence wavelengths were reached in the NIR region, and **TPhCN** had a longer wavelength of photoluminescence and lower quantum yield (QY) than **TPhNC** (**TPhCN:** λFLmax = 777 nm, Φ_{FL} = 1.0%, **TPhNC:** λFLmax = 768 nm, Φ_{FL} = 3.1%). The bathochromic wavelength shifts in absorption and PL spectra originating from the extension of the π-conjugated system were achieved by the π-extension of **TPh** with a narrow energy gap owing to the electronic effects of hypervalent tin. This suggests that hypervalent tin has the same electronic effects on the π-conjugated system in the dinuclear compounds for narrowing the energy gap as observed when the mononuclear compound is laddered. In the previous research by Peon *et al.*,[27] **TPh** derivatives are known to form bending structures by photoexcitation. In contrast, our dinuclear hypervalent compounds hardly showed such bending behaviors compared to the optimized structures in the ground and excited states (Fig. S8†). Therefore, the symmetric structures of the dinuclear compounds should contribute to the suppression of the structural relaxation by photoexcitation. In addition, the structural differences were hardly observed between the optimized structures of **TPhCN** and **TPhNC** in the ground and excited states (Fig. S8†). It is, therefore, implied that the difference in the Stokes shift could be attributed to the difference in the electronic state of each compound. These findings indicate that the transitional characteristics in MO exhibit different responses depending on the positions of dinucleation in the ladder structure.

The electronic states of π-conjugated molecules can be influenced by the direction of imine bonds and the positions of nitrogen atoms in forming the hypervalent state. We explored the electronic states and the impact of dinucleation by comparing the mononuclear and dinuclear hypervalent tin compounds (Fig. 4c, S9 and Tables S7, S8†). As depicted in Fig. 4c, **TPhCN** and **TPhNC** exhibited narrower energy gaps than **TPh** because of the extension of their π-conjugated scaffolds. Focusing on the range of changes in the MO levels compared to **TPh**, the HOMO of **TPhCN** is destabilized more significantly than that of **TPhNC** (**TPhCN**: −4.87 eV, **TPhNC**: −5.25 eV), and the LUMO of **TPhNC** is stabilized more dramatically than that of **TPhCN** (**TPhCN**: −2.54 eV, **TPhNC**: −2.97 eV). We considered that these are derived from the direction of the imine bonds. In **TPhCN**, the electron-donating effect of the two imine bonds contributed to the central benzene ring, which is expected to destabilize the HOMO by increasing the electron density. In **TPhNC**, on the other hand, the electron-withdrawing effect of the two imine bonds should stabilize the LUMO by promoting electron deficiency of the central benzene ring. Moreover, we assessed the MO energy levels using cyclic voltammetry (CV), as illustrated in Fig. S10.† The HOMO and LUMO energy levels of **TPh**, **TPhCN**, and **TPhNC** determined from the cyclic voltammograms closely mirrored the trends observed in the results from the DFT calculations. Notably, it was concluded that the positions of dinucleation in the ladder structure strongly affected the optical and electronic properties.

Open Access Article. Published on 10 October 2024. Downloaded on 2/15/2026 8:28:08 PM.
This article is licensed under a Creative Commons Attribution-NonCommercial 3.0 Unported Licence.

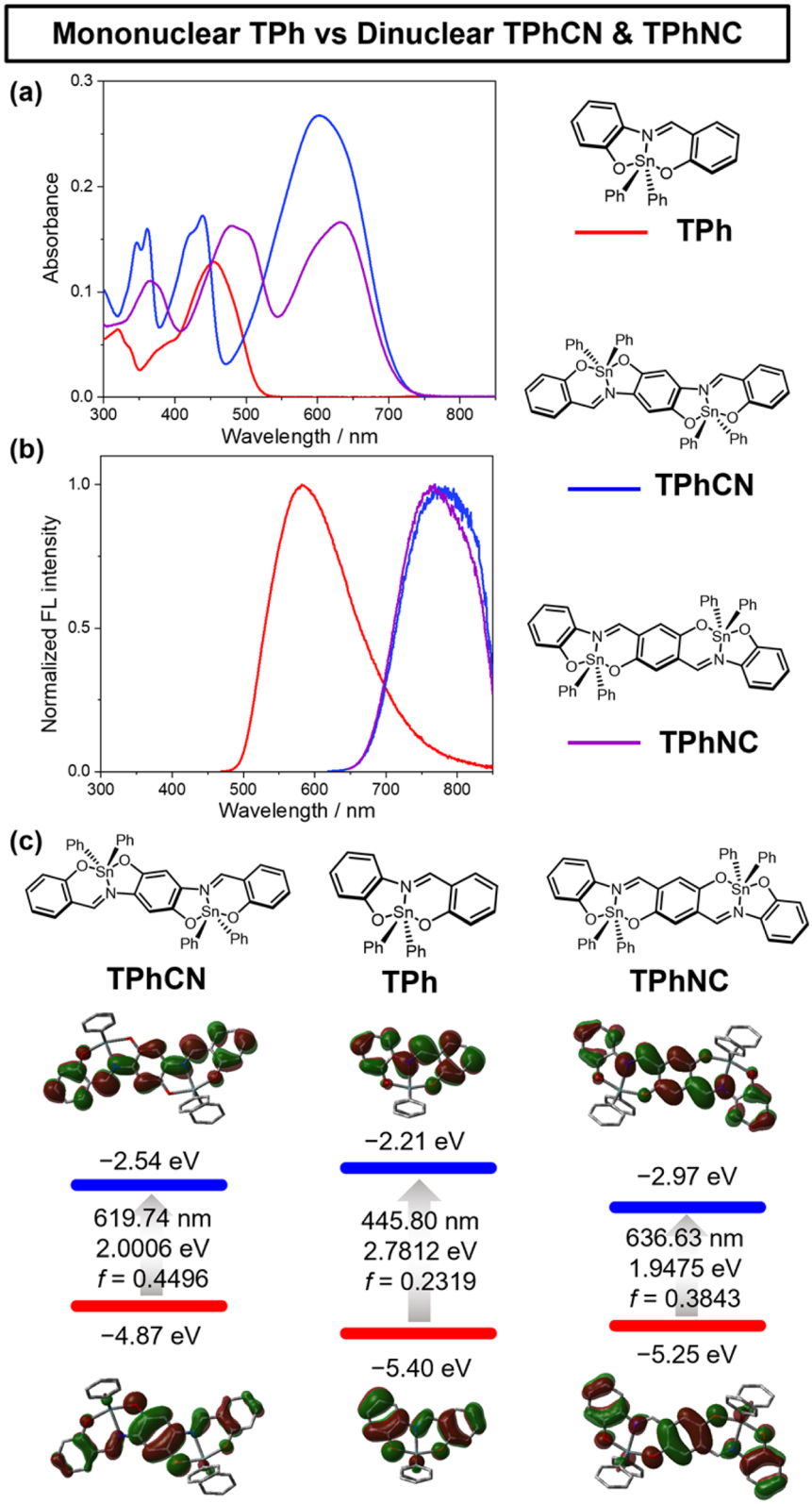

Fig. 4 (a) UV-vis absorption and (b) fluorescence spectra of **TPh**, **TPhCN**, and **TPhNC** in toluene (1.0×10^{-5} M). (c) Energy diagrams selected MOs and oscillator strengths (*f*) of selected transition bands of **TPh**, **TPhCN**, and **TPhNC** obtained with DFT and TD-DFT calculations at TD-B3LYP/6-31G(d)//B3LYP/6-31G(d) level for C, H, N, O, and LanL2DZ for Sn (isovalue = 0.02).

© 2024 The Author(s). Published by the Royal Society of Chemistry

Open Access Article. Published on 10 October 2024. Downloaded on 2/15/2026 8:28:08 PM. This article is licensed under a Creative Commons Attribution-NonCommercial 3.0 Unported Licence.

Table 1 Optical data of hypervalent compounds

	$\lambda_{abs}{}^{a}$/nm	$\varepsilon^{a}/10^4$ cm^{-1} M^{-1}	$\lambda_{FL}{}^{a}$/nm	$\Phi_{FL}{}^{b}$/%
TPh	454	1.29	584	28.0
TPhCN	604	2.68	777	1.0
TPhNC	632	1.61	768	3.1

[a] In toluene (1.0×10^{-5} M), excited at λ_{abs} for FL. [b] Absolute FL quantum yield, excited at 454 nm for **TPh** and at 525 nm for **TPhCN** and **TPhNC**.

The photoluminescence spectra of TPh derivatives in the solid state were observed and compared with those in the solution state (Fig. S11†). Focusing on the emission wavelengths, the change was hardly observed in **TPh** ($\lambda^{max}_{FL,solid}$ = 576 nm, $\Phi_{FL,solid}$ = 18.4%). This slight wavelength change should be due to the weak intermolecular interactions. On the other hand, the emission bands of both dinuclear compounds **TPhCN** and **TPhNC** were shifted to the longer wavelength regions, leading to their solid-state NIR luminescence (**TPhCN**: $\lambda^{max}_{FL,solid}$ = 836 nm, Φ_{FL} = 0.5%, **TPhNC**: $\lambda^{max}_{FL,solid}$ = 796 nm, $\Phi_{FL,solid}$ = 2.4%). Considering these results and the optimized structures in the ground and excited states, their symmetric structures should restrict structural relaxation. Consequently, we speculate that the observed emission in the longer wavelength region can be attributed to intermolecular interactions. The dinuclear compounds also exhibited aggregation-caused quenching properties that reduced the quantum yield.[31] These results suggest that the construction of symmetric structures affects not only the electronic state of the molecules but also their mobility.

We draw the MEP surface to examine the charge distribution of these hypervalent compounds (Fig. 5). **TPh** showed the unsymmetrical charge distribution, and the benzene ring of the N-side had a larger negative charge than that of the C-side, as described previously (Fig. 5a). In addition, reflecting the charge distribution of **TPh**, **TPhCN** had a large negative charge in the center benzene ring (Fig. 5b), while **TPhNC** had that in the side benzene rings (Fig. 5c). Therefore, this molecular design of dinucleation provided charge separation and quadrupolar molecules in the ground state, and **TPhCN** and **TPhNC** constituted the ring-fused A–π–D–π–A and the D–π–A–π–D systems, respectively.

The absorption spectra were measured in dichloromethane (CH_2Cl_2), chloroform ($CHCl_3$), toluene, and cyclohexane (c-hex) to gain insights into the solvent effects on these compounds. Surprisingly, both **TPhCN** and **TPhNC** exhibited negative solvatochromism in the only absorption property regardless of their neutral and symmetric structures. Meanwhile, the emission wavelengths hardly changed depending on those solvents (Fig. 5). In general, negative solvatochromism is caused by photoexcitation changes in the dipole moment.[32] However, the DFT calculations suggested that the dipole moments in **TPhCN** and **TPhNC** are almost identical (Fig. S12†). On the other hand, there are few examples of negative solvatochromism in the only absorption property because of "Symmetry breaking" in the ground state. Terenziani *et al.* predicted the existence of molecules with negative solvatochromism only in the absorption spectrum (referred to as "Class III" in the literature).[26,33,34] They proved that polymethine derivatives fall into this category.[33] These reports showed that large quadrupolar dyes caused negative solvatochromism in the only absorption property because the ground state was bistable (D–π–A$^-$–π–D$^+$ or D$^+$–π–A$^-$–π–D) and the excited state was stable as nonpolar. Therefore, we estimated the dinuclear compounds **TPhCN** and **TPhNC** have a large quadrupolar in the only ground state owing to the electronic effects unique to the hypervalent state and their imine moiety. We further observed the solvent effects in the DFT calculations. We reproduced the results, that is, the same as the tendency of optical measurements (Fig. S13,† the calculation was performed against CH_2Cl_2, $CHCl_3$, toluene, and c-hex). These findings propose that the electronic effects of hypervalent states can be exploited to create a novel D–A system in small molecules beyond the conventional D–A linking method.

Electronic properties of conjugated polymers using TPh, TPhCN and TPhNC

Optical measurements with polymers showed that **P-TPhCN** and **P-TPhNC** exhibited absorption and emission bands in longer wavelength regions than **P-TPh** (Fig. 6a and Table 2). It should be noted that the emission maximum wavelengths in **P-TPhCN** and **P-TPhNC** exceeded 800 nm (**P-TPh**: λ^{max}_{abs} = 518 nm, λ^{max}_{FL} = 621 nm, Φ_{FL} = 35.8%, **P-TPhCN**: λ^{max}_{abs} = 658 nm, λ^{max}_{FL} = 828 nm, Φ_{FL} = 0.3%, **P-TPhNC**: λ^{max}_{abs} = 683 nm, λ^{max}_{FL} = 801 nm, Φ_{FL} = 1.2%, 1.0×10^{-5} M in $CHCl_3$). Since the conjugated system of the dinuclear compound can also be extended by polymerization, followed by the bathochromic shifts of optical bands, it is shown that the dinuclear compounds are a promising building block for constructing NIR materials. The solvent effects on the optical properties were also investigated with the polymers (Fig. S14 and Table S10†). Shoulders, possibly due to aggregation, were observed from all polymers in cyclohexane. The change in the PL spectrum was observed only from **P-TPh**, and similar spectra were obtained from **P-TPhCN** and **P-TPhNC**. Moreover, similar shifts in the absorption wavelength were observed in **P-TPhCN** and **P-TPhNC**. These results imply that electronic structures of the monomers could be maintained in the polymer main-chains. In the film state, bathochromic wavelength shifts in the absorption and PL spectra, and the aggregation-caused quenching were observed from all polymers comparing to those of the solution state, possibly due to interactions between polymer chains (Fig. S15 and Table S11†).

The DFT calculations were performed to assess the extension of conjugation in mononuclear and dinuclear compounds with two and three units (Fig. 6b and S16–S21†). In the mononuclear compound, the HOMO and LUMO expanded as the number of units increased, whereas expansion of π-conjugation in the entire molecule was hardly observed, which might be attributed to the twisted bithiophene unit. In the A–π–D–π–A dinuclear compound **TPhCN**, as the number of units increased, the LUMO was expanded because of its high planarity, while the HOMO was localized in the dinuclear compound owing to the electron-rich moiety of the center benzene ring. On the other hand, in

Open Access Article. Published on 10 October 2024. Downloaded on 2/15/2026 8:28:08 PM.
This article is licensed under a Creative Commons Attribution-NonCommercial 3.0 Unported Licence.

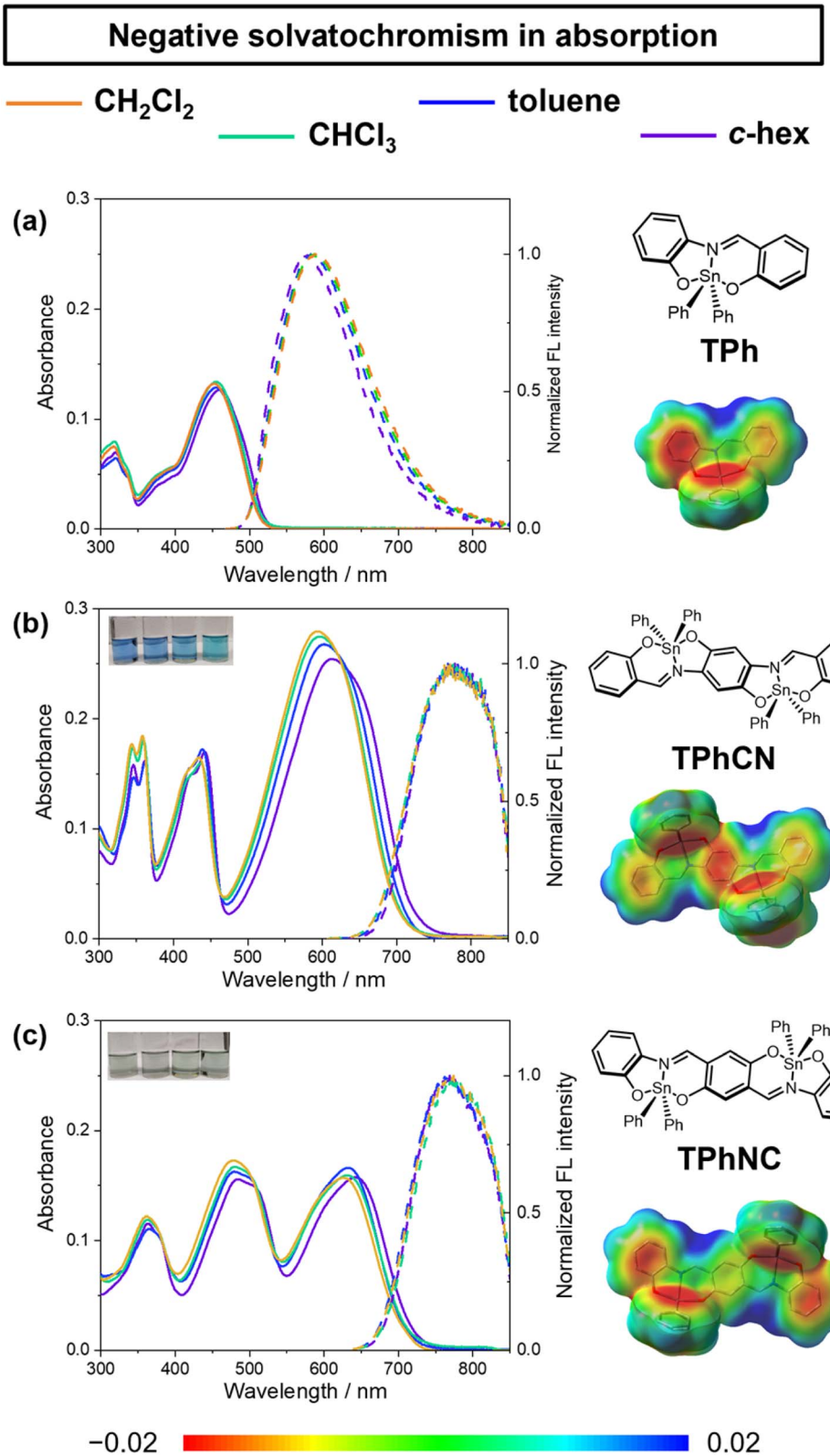

Fig. 5 Solvent-dependent UV-vis absorption and fluorescence spectra of (a) **TPh**, (b) **TPhCN**, and (c) **TPhNC** in each solvent (1.0×10^{-5} M, toluene/each solvent = 1/99 v/v). Inset: Molecular electrostatic potential (MEP) surface of each compound with DFT calculations at TD-B3LYP/6-31G(d)/level for C, H, N, O, and LanL2DZ for Sn (isovalue = 0.02).

© 2024 The Author(s). Published by the Royal Society of Chemistry

Open Access Article. Published on 10 October 2024. Downloaded on 2/15/2026 8:28:08 PM.
This article is licensed under a Creative Commons Attribution-NonCommercial 3.0 Unported Licence.

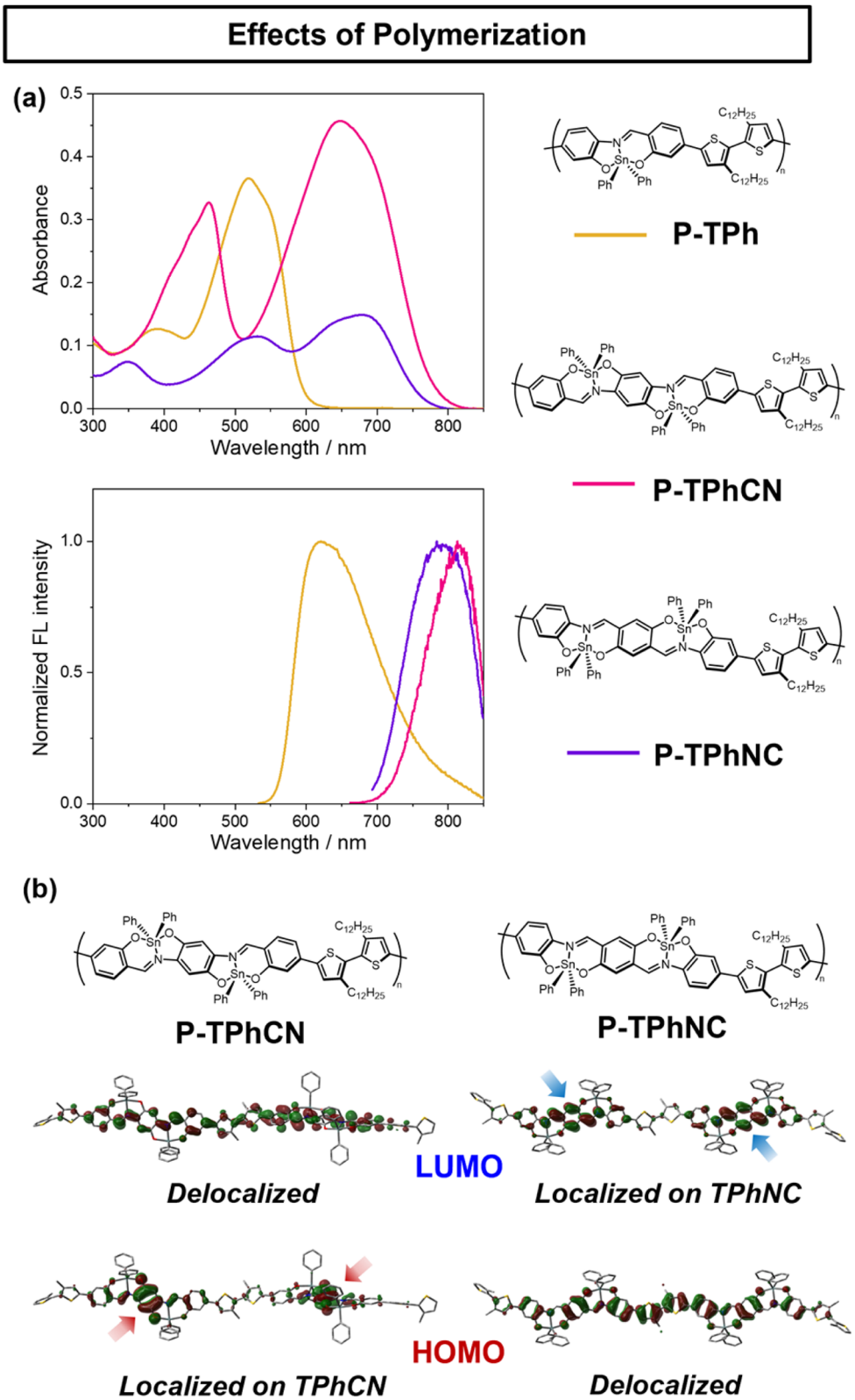

Fig. 6 (a) UV-vis absorption and fluorescence spectra of **P-TPh**, **P-TPhCN**, and **P-TPhNC** in $CHCl_3$ (1.0×10^{-5} M per repeating unit). (b) Molecular orbitals of **P-TPhCN**, and **P-TPhNC** (tri-units) at TD-B3LYP/6-31G(d)/level for C, H, N, O, S and LanL2DZ for Sn (isovalue = 0.02).

the D–π–A–π–D dinuclear compound **TPhNC**, the HOMO was extended throughout the main chain, and the LUMO was localized on the dinuclear compound unit because of the centered electron-deficient benzene ring. These results suggest that the charge distribution induced by each direction of dinucleation (**TPhCN** or **TPhNC**) leads to different orbitals in

Open Access Article. Published on 10 October 2024. Downloaded on 2/15/2026 8:28:08 PM. This article is licensed under a Creative Commons Attribution-NonCommercial 3.0 Unported Licence.

Table 2 Optical data of conjugated polymers

	$\lambda_{abs}{}^{a}$/nm	$\varepsilon^{a}/10^{4}$ cm^{-1} M^{-1}	$\lambda_{FL}{}^{a}$/nm	$\Phi_{FL}{}^{b}$/%
P-TPh	518	3.66	621	35.8
P-TPhCN	646	4.57	828	0.3
P-TPhNC	678	1.49	801	1.2

[a] In $CHCl_3$ (1.0×10^{-5} M per repeating unit), excited at λ_{abs} for FL. [b] Absolute FL quantum yield, excited at 518 nm for **P-TPh** and 525 nm for **P-TPhCN** and **P-TPhNC**.

the extended MOs, altering the energy level of each MO. As described above, polymerization of polarized D–π–A–π–D or A–π–D–π–A type molecules is suggested to induce specific orbital extensions, and the polarized state in π-conjugated scaffolds can be featured by constructing conjugated polymers.

Conclusion

By employing the electronic effects of hypervalent tin, we realized unique electronic structures and functions based on the ladderization of the π-conjugated Schiff base scaffold. In the mononuclear compound, the tin coordination enhanced the electron-withdrawing character in the inductive effect from the imine bond. As a result, the D–π–A structures were built without incorporating electron-donating units. This design strategy is useful in that it is simple and different from the usual D–A linkage and will be able to create additional molecular diversity by ligands and main group elements. Moreover, in the dinuclear compounds, we succeeded in synthesizing two kinds of compounds with NIR luminescence properties in the facile two-step procedure. These molecules showed the two types of quadrupolar, A–π–D–π–A and D–π–A–π–D, derived from two imine bonds and hypervalent tin in the molecule. Negative solvatochromism was observed in the absorption property originating from strong quadrupolar structures. Finally, conjugated polymerization of each molecule not only achieved luminescence in the NIR wavelength region over 800 nm because of the extended conjugation but also observed different orbital distributions on the polymer main chain originating from the electric charge distribution of the monomer. Our findings propose that the hypervalent atoms should be a promising tool for modulating the electronic structures of π-conjugated scaffolds followed by optical properties. This approach can be further developed by designing new ligands and diversifying the main group elements, which might be a platform for novel functional materials.

Data availability

ESI† available. Crystallographic data for **TPhCN** and **TPhNC** has been deposited at the CCDC under 2373875 and 2373876.

Author contributions

K. T. (Kazuya Tanimura) wrote the original draft, conducted the data analysis, and performed additional experiments. K. T. (Kento Tanaka) synthesized the compounds, performed the experiments, conducted the data analysis, and performed additional experiments. M. G. and K. T. (Kazuo Tanaka) supervised the project. All the authors discussed the results and contributed to editing the manuscript.

Conflicts of interest

There are no conflicts to declare.

Acknowledgements

This work was partially supported by the Hirose Foundation (for M. G.), a Grant-in-Aid for Scientific Research (B) (for M. G.) (JP22H02130 and JP23K23398) and (for K. T.) (JP24K01570).

References

1 A. Haque, K. M. Alenezi, M. S. Khan, W.-Y. Wong and P. R. Raithby, *Chem. Soc. Rev.*, 2023, **52**, 454–472.
2 Z. Zhang and Y. Li, *Angew. Chem., Int. Ed.*, 2021, **60**, 4422–4433.
3 D. Luo, W. Jang, D. D. Babu, M. S. Kim, D. H. Wang and A. K. K. Kyaw, *J. Mater. Chem. A*, 2022, **10**, 3255–3295.
4 D. Meng, R. Zheng, Y. Zhao, E. Zhang, L. Dou and Y. Yang, *Adv. Mater.*, 2022, **34**, 2107330.
5 G. Feng, G.-Q. Zhang and D. Ding, *Chem. Soc. Rev.*, 2020, **49**, 8179–8234.
6 V. K. Praveen, B. Vedhanarayanan, A. Mal, R. K. Mishra and A. Ajayaghosh, *Acc. Chem. Res.*, 2020, **53**, 496–507.
7 J. Lee, A. J. Kalin, T. Yuan, M. Al-Hashimi and L. Fang, *Chem. Sci.*, 2017, **8**, 2503–2521.
8 A. Fukazawa and S. Yamaguchi, *Chem.–Asian J.*, 2009, **4**, 1386–1400.
9 M. Stolar and T. Baumgartner, *Chem. Commun.*, 2018, **54**, 3311–3322.
10 T. Delouche, M. Hissler and P.-A. Bouit, *Coord. Chem. Rev.*, 2022, **464**, 214553.
11 J. I. Musher, *Angew. Chem., Int. Ed.*, 1969, **8**, 54–68.
12 R. Kumar, T. Dohi and V. V Zhdankin, *Chem. Soc. Rev.*, 2024, **53**, 4786–4827.
13 K. Tamao, *J. Synth. Org. Chem.*, 1990, **48**, 457–462.
14 K. Akiba, *Heteroat. Chem.*, 2009, **20**, 232–234.
15 J. Hyvl, *Dalton Trans.*, 2023, **52**, 12597–12603.
16 M. Gon, S. Ito, K. Tanaka and Y. Chujo, *Bull. Chem. Soc. Jpn.*, 2021, **94**, 2290–2301.
17 M. Gon, K. Tanaka and Y. Chujo, *Chem.–Eur. J.*, 2021, **27**, 7561–7571.
18 M. Gon, K. Tanimura, M. Yaegashi, K. Tanaka and Y. Chujo, *Polym. J.*, 2021, **53**, 1241–1249.
19 M. Gon, Y. Morisaki, K. Tanimura, K. Tanaka and Y. Chujo, *Mater. Chem. Front.*, 2023, **7**, 1345–1353.
20 M. Gon, T. Kato, K. Tanimura, C. Hotta and K. Tanaka, *RSC Mechanochemistry*, 2024, **1**, 322–327.
21 M. Gon, Y. Morisaki, K. Tanimura and K. Tanaka, *Dalton Trans.*, 2024, **53**, 11858–11866.

© 2024 The Author(s). Published by the Royal Society of Chemistry

Open Access Article. Published on 10 October 2024. Downloaded on 2/15/2026 8:28:08 PM.
This article is licensed under a Creative Commons Attribution-NonCommercial 3.0 Unported Licence.

22 M. Gon, M. Yaegashi, K. Tanaka and Y. Chujo, *Chem.–Eur. J.*, 2023, **29**, e202203423.
23 M. Gon, M. Yaegashi and K. Tanaka, *Bull. Chem. Soc. Jpn.*, 2023, **96**, 778–784.
24 K. Tanimura, M. Gon and K. Tanaka, *Inorg. Chem.*, 2023, **62**, 4590–4597.
25 M. Gon, K. Tanaka and Y. Chujo, *Polym. J.*, 2023, **55**, 723–734.
26 F. Terenziani, A. Painelli, C. Katan, M. Charlot and M. Blanchard-Desce, *J. Am. Chem. Soc.*, 2006, **128**, 15742–15755.
27 J. S. Zugazagoitia, M. Maya, C. Damián-Zea, P. Navarro, H. I. Beltran and J. Peon, *J. Phys. Chem. A*, 2010, **114**, 704–714.
28 S. Ohtani, M. Nakamura, M. Gon, K. Tanaka and Y. Chujo, *Chem. Commun.*, 2020, **56**, 6575–6578.
29 A. A. Diamantis, J. M. Gulbis, M. Manikas and E. R. T. Tiekink, *Phosphorus, Sulfur Silicon Relat. Elem.*, 1999, **150**, 251–259.
30 A. G. Blackman, E. B. Schenk, R. E. Jelley, E. H. Krenske and L. R. Gahan, *Dalton Trans.*, 2020, **49**, 14798–14806.
31 S. A. Jenekhe and J. A. Osaheni, *Science*, 1994, **265**, 765–768.
32 S. Nigam and S. Rutan, *Appl. Spectrosc.*, 2001, **55**, 362A–370A.
33 F. Terenziani, O. V. Przhonska, S. Webster, L. A. Padilha, Y. L. Slominsky, I. G. Davydenko, A. O. Gerasov, Y. P. Kovtun, M. P. Shandura, A. D. Kachkovski, D. J. Hagan, E. W. Van Stryland and A. Painelli, *J. Phys. Chem. Lett.*, 2010, **1**, 1800–1804.
34 C. Sissa, F. Delchiaro, F. Di Maiolo, F. Terenziani and A. Painelli, *J. Chem. Phys.*, 2014, **141**, 164306.